Cell Reports
Article

Insulin/IGF-1 Signaling Regulates Proteasome Activity through the Deubiquitinating Enzyme UBH-4

Olli Matilainen,[1,2] Leena Arpalahti,[1,2] Ville Rantanen,[2,3] Sampsa Hautaniemi,[2,3] and Carina I. Holmberg[1,2,*]
[1]Research Programs Unit, Translational Cancer Biology Program
[2]Institute of Biomedicine, Biochemistry and Developmental Biology
[3]Research Programs Unit, Genome Scale Biology Program
Biomedicum Helsinki, University of Helsinki, FI-00290 Helsinki, Finland
*Correspondence: carina.holmberg@helsinki.fi
http://dx.doi.org/10.1016/j.celrep.2013.05.012

SUMMARY

The proteasome plays an important role in proteostasis by carrying out controlled protein degradation in the cell. Impairments in proteasome function are associated with severe and often age-related diseases. Here, we have characterized a molecular mechanism linking insulin/IGF-1 signaling (IIS) to proteasome activity. We show that decreased IIS, which promotes proteostasis and longevity, increases proteasome activity through the FOXO transcription factor DAF-16 in *C. elegans*. Furthermore, we reveal that DAF-16 represses expression of the proteasome-associated deubiquitinating enzyme *ubh-4*, which we suggest functions as a tissue-specific proteasome inhibitor. Finally, we demonstrate that proteasome activation through downregulation of the *ubh-4* human ortholog *uchl5* increases degradation of proteotoxic proteins in mammalian cells. In conclusion, we have established a mechanism by which the evolutionarily conserved IIS contributes to the regulation of proteasome activity in a multicellular organism.

INTRODUCTION

Maintenance of protein homeostasis is essential to all living organisms. As an important part of the proteostasis network, the ubiquitin-proteasome system (UPS) executes most of the controlled protein degradation in the cell. In the UPS, the substrate protein targeted for degradation becomes polyubiquitinated via the actions of the ubiquitin-activating E1 enzyme, conjugating E2 enzymes, and ligating E3 enzymes (Hershko and Ciechanover, 1998). The polyubiquitinated substrate is then recognized and degraded by the 26S proteasome, a large multisubunit protein complex consisting of a 20S core capped by one or two regulatory 19S lid particles. The 20S core is a barrel-shaped complex of 28 subunits (14 α and 14 β subunits), and it contains the proteolytic activities of the proteasome, whereas the 19S regulatory particle, responsible for capture, deubiquitination, and unfolding of the polyubiquitinated substrates, forms from 19 different subunits. In addition, there are multiple proteasome-associated proteins possessing essential activities, such as ubiquitin ligases and deubiquitinating enzymes (DUBs), which regulate proteasome function (Finley, 2009; Hanna and Finley, 2007). The 20S can also be activated by the 11S complexes and PA200/Blm10 to promote degradation, probably mainly in an ubiquitin-independent manner (Stadtmueller and Hill, 2011). Thus, the proteasome is not a static proteolytic machine; on the contrary, its function is highly regulated (Finley, 2009; Hanna and Finley, 2007). However, it remains an open question how proteasome activity is regulated in a multicellular organism.

Dysfunction of the proteasome has been detected in many severe disorders, such as Alzheimer's, Parkinson's, and Huntington's diseases (Dahlmann, 2007), which usually emerge at the later stages of life. Accordingly, it has been postulated mainly based on in vitro proteasome activity assays that proteasomal degradation decreases upon aging. This might be due to reduced expression of proteasome subunits, a decrease in proteasome assembly, modifications of proteasome subunits, and/or inhibitory effects of oxidized and crosslinked substrates (Vernace et al., 2007). Additionally, the association and function of different proteasome regulators might change upon aging. Interestingly, an inhibitory mechanism seems to be part of the proteasome regulation and not only a physiological effect caused by aging, as the proteasome-associated DUB USP14 and its yeast ortholog Ubp6 have been shown to inhibit the proteasome (Hanna et al., 2006; Lee et al., 2010).

We have previously shown that proteasome activity changes upon aging in *C. elegans* (Hamer et al., 2010). This led us to ask whether signaling pathways regulating longevity also affect proteasome activity. Insulin/IGF-1 signaling (IIS) is an evolutionarily conserved signaling cascade regulating lifespan in worms, flies, rodents, and possibly humans (Kenyon, 2005, 2010). In *C. elegans*, reduced IIS caused by mutations in DAF-2 (insulin/IGF-1 receptor ortholog) leads to long-lived and stress-resistant worms (Kenyon et al., 1993), mediated through negative regulation of the FOXO transcription factor DAF-16 (Lin et al., 1997, 2001; Ogg et al., 1997). DAF-16 controls expression of multiple genes regulating diverse processes such as metabolism, stress responses, longevity, and development (Lee et al., 2003; Murphy et al., 2003). Decreased IIS also affects protein homeostasis during the normal aging process (Ben-Zvi et al., 2009; David et al., 2010) and under disease-related conditions (Cohen et al., 2006, 2009; Hsu et al., 2003; Morley et al., 2002).

In the current study, we demonstrate that proteasome activity is modified through the IIS and the proteasome-associated DUB

UBH-4. Our data show that DAF-16 negatively affects *ubh-4* expression. In line with being one of the many DAF-16 targets genes, our data reveal that *ubh-4* has a mild effect on *C. elegans* longevity. Furthermore, our results demonstrate that knockdown of *uchl5*, the mammalian ortholog of *ubh-4*, leads to increased degradation of proteins linked to proteotoxicity. Hence, we have established a molecular mechanism connecting the evolutionarily conserved IIS pathway to DUB-regulated proteasome activity.

RESULTS

IIS-Deficient *daf-2* Mutants Display Higher UPS Activity than Wild-Type Animals

Aging causes a decline in protein homeostasis leading to accumulation of damaged and unfolded proteins. An increasing body of evidence suggests that the same signaling pathways that are involved in controlling aging, including IIS, also regulate the mediators of proteostasis, such as metabolic enzymes, stress proteins, and chaperones (Balch et al., 2008). Here, we investigate whether IIS also contributes to regulation of the UPS by using the well-established aging model *C. elegans*. We have previously developed an in vivo reporter system for UPS activity based on the photoconvertible UbG76V-Dendra2 reporter protein (Hamer et al., 2010; Li et al., 2011), which allows us to measure the rate of proteasomal degradation in live animals. Because the intestine is an important tissue for DAF-16-mediated longevity in *C. elegans* (Libina et al., 2003), we initially imaged UPS activity in intestinal cells. The photoconverted UbG76V-Dendra2 signal decreased by approximately 30% in 6 hr in wild-type animals compared to an approximately 2-fold faster degradation in the long-lived *daf-2(e1370)* mutants (Figures 1A and 1B; Tables S1 and S2) without an effect on the control Dendra2 (Figures S1A and S1B). RNAi against proteasome 19S subunit *rpn-2* decreased the degradation of UbG76V-Dendra2 in the intestine of *daf-2(e1370)* mutants (Figure 1C), whereas RNAi of autophagy component *lgg-1* did not affect reporter degradation (Figure S1D), demonstrating that the reporter was proteasomally degraded in these animals. The enhanced UPS activity detected upon decreased IIS was DAF-16 dependent, as the effect was diminished in the *daf-16(m26);daf-2(e1370)* double mutant (Figures 1A and 1B). The short-lived *daf-16(m26)* or *daf-16(mgDf50)* mutants, deficient in five or all eight DAF-16 isoforms (Kwon et al., 2010; Lin et al., 1997; Ogg et al., 1997), showed similar reporter degradation as wild-type animals (Figure 1B). Together, these results demonstrate that under conditions of reduced IIS, active DAF-16 is mediating the enhanced UPS activity in the intestine.

We have previously shown that UPS reporter degradation is relatively slow in body-wall muscle cells (Hamer et al., 2010), and in line with this observation both the wild-type and *daf-2(e1370)* animals showed similar UbG76V-Dendra2 degradation of about 10% at 6 hr after photoconversion (data not shown). However, in 24 hr body-wall muscle cells of the *daf-2(e1370)* mutants exhibited a significantly faster UPS reporter degradation (approximately 1.2-fold) compared to wild-type animals (Figures 1D and S1C), which was not dependent on autophagy (Figure S1E). In contrast to the degradation in intestinal cells, the *daf-16(m26);daf-2(e1370)* or *daf-16(mgDf47);daf-2(e1370)* double mutations did not significantly decrease the reporter degradation rate (Figure 1D), suggesting that the enhanced degradation does not require active DAF-16 in body-wall muscle cells. Interestingly, *daf-16(m26)* mutants (deficient in five DAF-16 isoforms) displayed similar reporter degradation in body-wall muscle cells as the *daf-2(e1370)* mutants (Figure 1D). This appeared to be a muscle-specific function of the DAF-16 isoforms, because in *daf-16(mgDf50)* mutants (deficient in all DAF-16 isoforms) degradation was comparable to wild-type animals (Figure 1D). Altogether, reduced IIS leads to a minor increase in UPS activity also in body-wall muscle cells, but in a DAF-16-independent manner.

The proteasomal degradation of the UbG76V-Dendra2 UPS reporter is likely affected by specific ubiquitin ligase(s). Therefore, we have developed a fluorescent reporter that responds to changes in proteasome activity by detecting the pool of polyubiquitinated proteins in vivo. The reporter takes advantage of a commercially available short-lived fluorescent ZsProSensor fusion protein, which consists of ZsGreen fused to the C-terminal part of the mouse ornithine decarboxylase, a protein domain mediating proteasomal degradation in an ubiquitin-independent manner (Murakami et al., 1992). In line with being a proteasomal substrate, expression of the ZsProSensor in intestinal cells did not produce a fluorescent signal, suggesting that it is rapidly degraded in *C. elegans* (data not shown). We hypothesized that fusing the ZsProSensor to the ubiquitin interaction motifs (UIMs) of the proteasome 19S subunit RPN-10 would create a reporter that binds polyubiquitinated proteins via its UIM motifs, resulting in stabilization of the reporter and detectable fluorescence. Approaches using the polyubiquitin-binding domains have been reported for capturing the cellular pool of polyubiquitin chains from mammalian cell lysates (Bennett et al., 2007) and for visualizing polyubiquitinated proteins in mammalian cells (Sims et al., 2012). Expression of our polyubiquitin reporter in the *C. elegans* intestine resulted in visible fluorescent foci with a colocalizing pattern to immunostained polyubiquitinated proteins (Figure S2A). As we predicted, the polyubiquitin reporter also responded to proteasome dysfunction, as RNAi against *rpn-2* generated 2.6-fold higher fluorescent signal compared to control RNAi-treated animals (Figure S2B), thus validating the function of this in vivo polyubiquitin reporter system. The change in fluorescence intensity is likely dependent on both the UIM domains and the ZsProSensor degron, as upon proteasome impairment we would expect less degron-mediated degradation of the reporter resulting in increased fluorescence, as well as an increase in cellular polyubiquitinated proteins, which would create more binding sites for the polyubiquitin reporter and result in increased reporter fluorescence. Thus, the polyubiquitin reporter stability is affected by the balance between proteasomal degradation and binding to polyubiquitinated proteins. By using the polyubiquitin reporter approach, we were able to confirm the importance of DAF-16 in enhancing proteasomal degradation in the intestine, as *daf-16* RNAi increased the fluorescent intensity in the *daf-2(e1370)* background, but not in wild-type animals (Figure 2). These results further demonstrate that IIS has a crucial role in regulating proteasome activity in vivo.

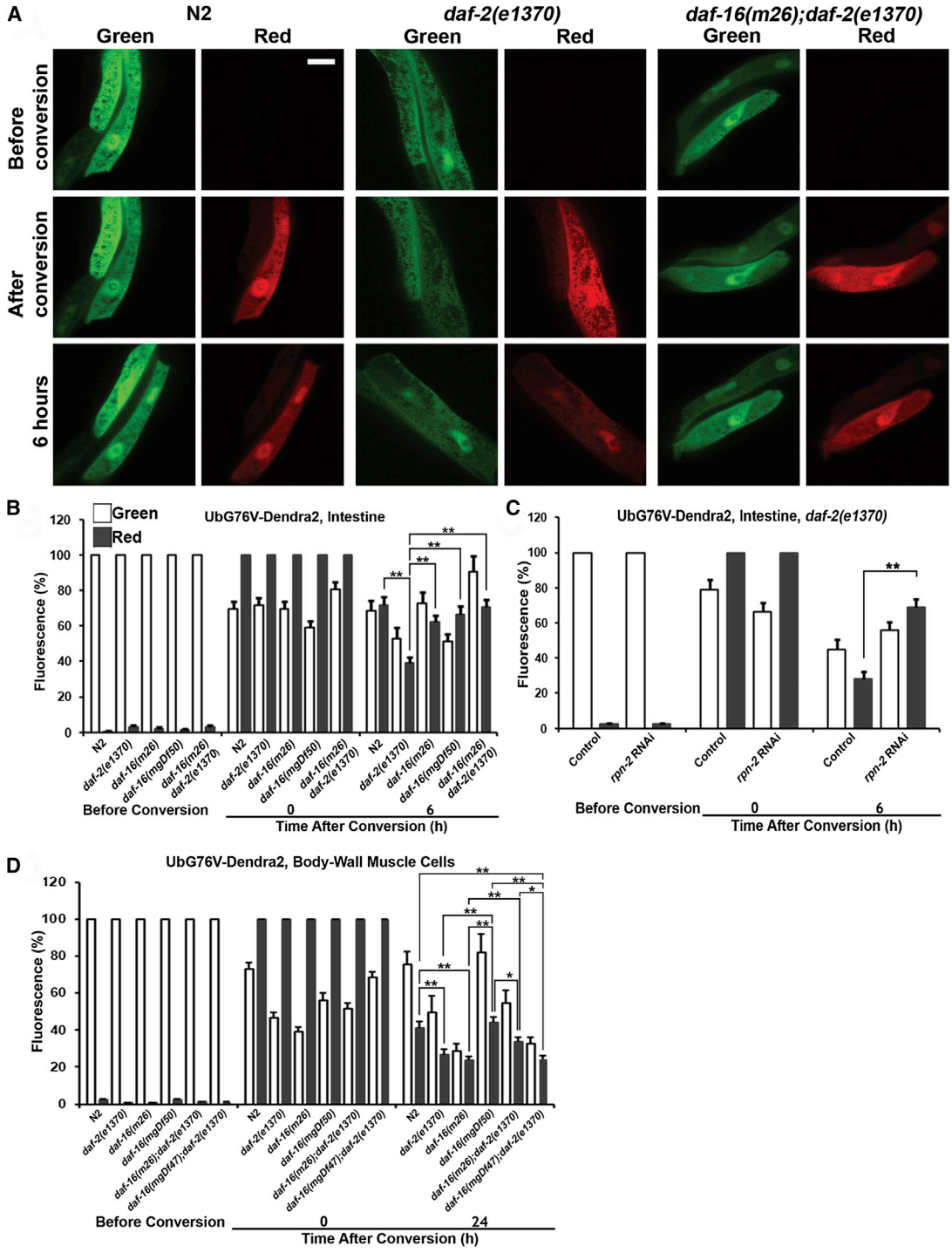

Figure 1. Reduced IIS Increases UPS Activity In Vivo

(A) Fluorescence micrographs of wild-type, *daf-2(e1370)*, and *daf-16(m26);daf-2(e1370)* animals expressing UbG76V-Dendra2 in intestinal cells before, after, and 6 hr after photoconversion.

(B) Quantification of UbG76V-Dendra2 degradation in intestinal cells of wild-type and IIS mutant animals.

(C) Quantification of UbG76V-Dendra2 degradation in intestinal cells of *daf-2(e1370)* animals after control or *rpn-2* RNAi.

(D) Quantification of UbG76V-Dendra2 degradation in body-wall muscle cells of wild-type and IIS mutant animals. All graphs show the average percentage of green or red fluorescence relative to the initial fluorescence intensity (before photoconversion) or the intensity at the point of photoconversion (0 hr after conversion), respectively.

Scale bar 20 μm. Error bars, SEM, *p < 0.05 and **p < 0.01, Table S2. See also Figure S1.

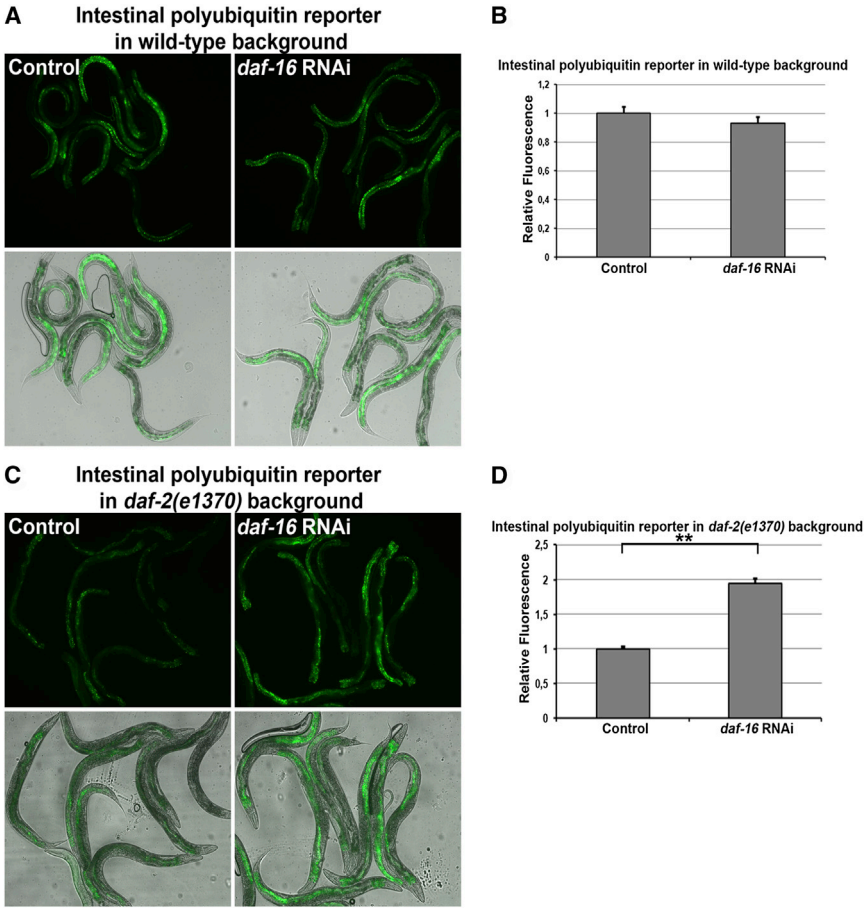

Figure 2. IIS Affects the Stability of the Intestinal Polyubiquitin Reporter

(A) Fluorescence micrographs of control or *daf-16* RNAi-treated wild-type animals expressing the polyubiquitin reporter (*Pvha-6::UIM2-ZsPro-Sensor*) in the intestine.

(B) Quantification of the fluorescent intensity of the intestinal polyubiquitin reporter in wild-type animals after control or *daf-16* RNAi.

(C) Fluorescence micrographs of control or *daf-16* RNAi-treated *daf-2(e1370)* animals expressing the polyubiquitin reporter (*Pvha-6::UIM2-ZsPro-Sensor*) in the intestine. Exposure time used for green fluorescent channel is longer in (A) than in (C).

(D) Quantification of the fluorescent intensity of the intestinal polyubiquitin reporter in *daf-2(1370)* animals after control or *daf-16* RNAi. Graphs show average fold change in fluorescence compared to the control RNAi (set as 1). Error bars, SEM, $^{**}p < 0.01$, Table S2.

See also Figure S2.

To complement the in vivo approaches, we also investigated proteasome activity in whole-animal lysates (Figure 3A) using the well-known native in-gel proteasome activity assay with suc-LLVY-AMC-substrate (Elsasser et al., 2005), which enables visualization of active proteasome complexes. We observed that *daf-2(e1370)* mutants displayed approximately 1.6-fold higher proteasome activity compared to wild-type animals (Figure 3B), which is similar to the in vivo UPS reporter data (Figures 1A and 1B). The increase in activity was diminished in *daf-16(m26);daf-2(e1370)* double mutants (Figure 3B), further demonstrating that activation of DAF-16 through decreased IIS enhances proteasome activity. Proteasome activity was slightly increased in lysates from *daf-16(m26)* mutants (Figure 3B), which parallels the observation in body-wall muscle cells (Figure 1D) and show that the in vitro assay reflects the sum of proteasome activity. Taken together, both our in vivo and in vitro results demonstrate that the reduced IIS in long-lived *daf-2(e1370)* mutants enhances proteasome activity. Notably, a recent article (Vilchez et al., 2012b) stated that reduced IIS does not upregulate proteasome activity based on in vitro proteasome peptidase assay with whole-animal lysates from the sterile *daf-2(mu150);fer-15(b26);fem-1(hc17)* mutant strain. The differences in genetic background of the *daf-2* animals and in the specificity of the in vitro assays used most likely explain the different outcome compared to our study.

Our observed increase in proteasome activity in *daf-2(e1370)* mutants could arise from differences in proteasome abundance. However, no difference in the proteasome amount was detected between wild-type and IIS mutant animals by western blotting against the proteasome 20S alpha subunits (Figures 3C and 3D). Our result is in agreement with previous microarray and quantitative mass spectrometry data, showing that proteasome subunits are not more highly expressed in *daf-2* mutants than in wild-type animals (Dong et al., 2007; McElwee et al., 2003; Murphy et al., 2003; Zarse et al., 2012). Thus, the enhanced UPS activity detected upon decreased IIS in *C. elegans* is not derived from changes in proteasome levels, but rather from differences in the regulation of its function.

UBH-4 Is a Proteasome-Associated DUB in *C. elegans*

We hypothesized that there might be differences in the composition of the proteasome regulatory complexes between wild-type and *daf-2(e1370)* animals. We therefore analyzed RP_2-core particle (CP) and RP-CP complexes isolated from native gel with LC-MS-MS and detected most of the 19S regulatory particles in both wild-type and *daf-2(e1370)* samples (Table S3). Variations in 19S RP composition or in the associated proteins may lead to differences in proteasome activity. Interestingly, the deubiquitinating enzyme (DUB) UBH-4 was detectable in wild-type, but not in *daf-2(e1370)* samples. UBH-4 has previously been shown to interact with the 19S subunit RPN-13 by yeast two-hybrid experiment (Li et al., 2004) and the mammalian homolog UCHL5 to associate with RPN13 (Hamazaki et al., 2006; Qiu et al., 2006; Yao et al., 2006). To investigate the in vivo interaction in *C. elegans*, we expressed His- and streptavidin-binding-protein (SBP)-tagged UBH-4 and HA-tagged RPN-13 under their own promoters. Immunoprecipitation of

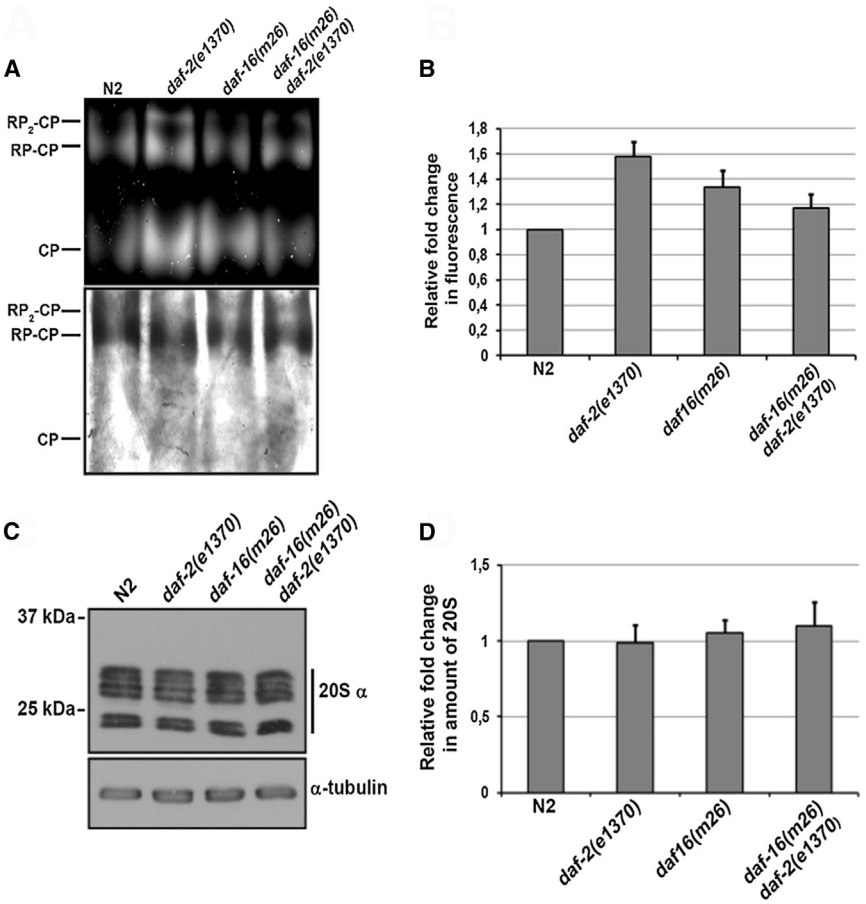

Figure 3. Reduced IIS Increases Proteasome Activity In Vitro without Affecting Proteasome Amount

(A) Lysates of wild-type and IIS mutant animals separated on a native gel followed by in-gel proteasome activity assay with fluorogenic suc-LLVY-AMC substrate. Lower panel shows Coomassie staining of the gel. RP-CP and RP_2-CP refer to proteasome 20S CP capped at one or both ends with 19S RP, respectively.

(B) Quantification of proteasome in-gel activity from wild-type and IIS mutant animals. Graph shows the average fold changes compared to the wild-type (set as 1). The quantification is the sum of fluorescent signal within RP_2-CP, RP-CP, and CP. Results are mean of quantifications of independent experiments (N2 and *daf-2[e1370]* n = 21, *daf-16[m26]* n = 17 and *daf-16[m26];daf-2[e1370]* n = 16). Error bars, SEM.

(C) Lysates of wild-type and IIS mutant animals immunoblotted against proteasome 20S alpha subunits.

(D) Quantification of the proteasome immunoblots. Graph shows the average fold changes compared to the wild-type (set as 1). Results are mean of quantifications (n = 3 independent experiments for all strains). Error bars, SEM.

His-SBP-UBH-4, but not His-SBP-GFP, brought down HA-RPN-13 (Figure 4A), demonstrating that UBH-4 and RPN-13 interact in *C. elegans*.

To confirm the DUB function of UBH-4 in *C. elegans*, we downregulated UBH-4 by RNAi and analyzed the proteasome-associated DUB activity with in-gel activity assay. To specifically detect the proteasome-associated DUB activity, only the part of the native gel containing the RP2-CP and RP-CP complexes was incubated with the Ub-AMC substrate. A clear reduction in fluorescence, i.e., substrate hydrolysis, which reflects decreased deubiquitinating activity, was detected in lysates of *ubh-4* RNAi-treated animals compared to control lysates, establishing that UBH-4 functions as a DUB in *C. elegans* (Figure 4B). Additionally, we observed accumulation of polyubiquitinated proteins after *ubh-4* RNAi (Figures 4C and 4D), suggesting that the deubiquitinating activity of UBH-4 is required to maintain protein homeostasis.

Expression of *ubh-4* Is Negatively Regulated by DAF-16

As we detected UBH-4 in lysates from wild-type, but not *daf-2(e1370)* mutant animals in the mass spectrometry analysis, we speculated that the expression of *ubh-4* may be regulated through IIS. To examine the transcriptional regulation of *ubh-4*, we expressed GFP under the *ubh-4* promoter and 3′ UTR. GFP was detected in several tissues such as the muscles and neurons, with the highest expression being in the intestine (Figure 5A). The *ubh-4* expression decreased upon aging but without notable changes in the expression pattern (Figures S3A and S3B). Interestingly, a clear difference between wild-type and *daf-2(e1370)* mutants was a high GFP expression in the intestine of young adult wild-type animals (Figure 5A, left panels), hardly detectable in the *daf-2(e1370)* mutants (Figure 5A, middle left panels). In turn, *daf-2(e1370)* mutants displayed higher GFP expression in embryos than the wild-type animals (Figure 5A, middle left panels). *daf-16(m26)* and *daf-16(m26);daf-2(e1370)* mutants showed similar expression pattern as the wild-type animals with a strong GFP signal in the intestine (Figure 5A, right middle and right panels, respectively). Taken together, these data suggest that DAF-16 negatively regulates *ubh-4* expression in the intestine. Because different DAF-16 isoforms regulate expression of partly distinct sets of genes (Kwon et al., 2010), we also investigated the expression of *Pubh-4::gfp* in *daf-16* deletion mutants in addition to the *daf-16(m26)* point mutation. In both *daf-16(mgDf50)* and *daf-16(mgDf47);daf-2(e1370)* deletion mutants, the GFP expression pattern resembled wild-type with high intestinal expression (Figure S4A). To further confirm the DAF-16-dependent regulation of *ubh-4* expression in the intestine, we downregulated DAF-16 by RNAi in *daf-2(e1370)* animals expressing *Pubh-4::gfp*. *daf-16* RNAi clearly increased the GFP signal in the intestine of *daf-2(e1370)* mutants (Figure S4B), demonstrating that *ubh-4* expression is negatively regulated by DAF-16 in the intestine of *C. elegans*. The DAF-16a and DAF-16d/f isoforms have been connected to lifespan regulation (Kwon et al., 2010; Lee et al., 2001; Lin et al., 2001), and we therefore performed

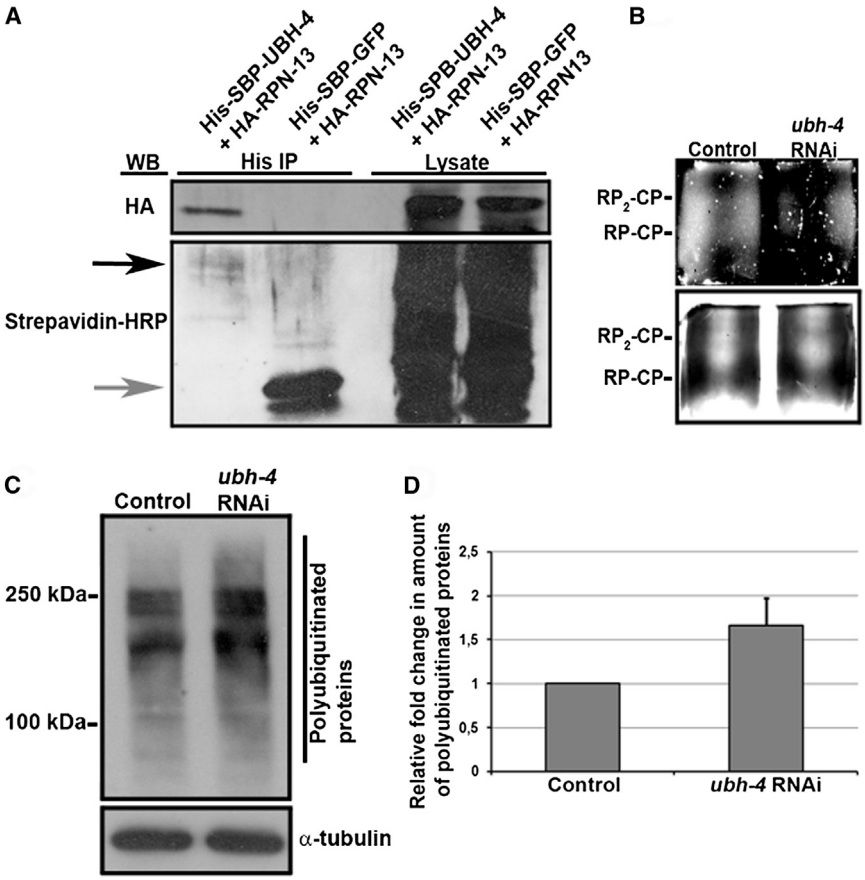

Figure 4. UBH-4 Interacts with RPN-13 and Functions as a DUB in *C. elegans*

(A) Immunoprecipitation of HA-RPN-13 with His-SBP-UBH-4 or His-SBP-GFP (control) from whole-animal lysates followed by western blotting with anti-HA and streptavidin-HRP antibodies. Black arrow indicates His-SBP-UBH-4 and gray arrow His-SBP-GFP band.

(B) Lysates of *rrf-3(pk1426)* animals treated with control or *ubh-4* RNAi separated on a native gel followed by in-gel DUB activity assay. Only the part of the native gel containing the RP2-CP and RP-CP was incubated with the fluorogenic Ub-AMC substrate. Note that the bands corresponding to the RP2-CP and RP-CP tend to diffuse in the native gel. Lower panel shows Coomassie staining of the same gel piece.

(C) Lysates of *rrf-3(pk1426)* animals treated with control or *ubh-4* RNAi immunoblotted against polyubiquitinated proteins.

(D) Quantification of polyubiquitinated protein amount. Graph shows the average fold change compared to the control RNAi (set as 1). Results are mean of quantifications (control and *ubh-4* RNAi n = 14 independent experiments). Error bars, SEM.

DAF-16 isoform-specific RNAi. Both downregulation of *daf-16a* and *daf-16d/f* induced an upregulation of *Pubh-4::gfp* expression in the intestine of *daf-2(e1370)* mutants (Figure S4C), suggesting that multiple DAF-16 isoforms are regulating *ubh-4* expression. We identified one canonical DAF-16 binding site (GTAAACA, Furuyama et al., 2000) on the proximal promoter (531–525 bp upstream from first coding codon) of *ubh-4*. This site is also contained within the modENCODE reported DAF-16 binding region defined by chromatin immunoprecipitation sequencing (ChIP-seq) of a DAF-16::GFP fusion protein (Celniker et al., 2009) (Figure S4D). We mutated the canonical DAF-16 binding site on *Pubh-4::gfp* expression vector and observed a clear increase in intestinal GFP expression in *daf-1(e1370)* animals (Figure 5B), suggesting that DAF-16 regulates *ubh-4* expression from its canonical binding site on the *ubh-4* promoter.

The overall *ubh-4* expression was downregulated by 20% in *daf-2(e1370)* mutants compared to wild-type animals when analyzed by quantitative PCR (qPCR) (Figure 5C). However, *daf-16(m26)* and *daf-16(m26);daf-2(e1370)* double mutants showed similar levels of *ubh-4* mRNA compared to wild-type animals (Figure 5C), providing further support for the observation that DAF-16 negatively regulates *ubh-4* expression. To test whether we could mimic the *ubh-4* expression level detected in *daf-2(e1370)* mutants, we performed *ubh-4* RNAi dilution experiments. *ubh-4* RNAi produced an approximately 80% decrease in *ubh-4* mRNA levels (Figure 5D). By diluting *ubh-4* RNAi bacteria to a final concentration of 1% with bacteria carrying an empty plasmid (*pL4440*), we were able to decrease *ubh-4* mRNA levels by 20%, which is comparable to the level observed in *daf-2(e1370)* mutants (Figures 5C and 5D). Furthermore, diluted *ubh-4* RNAi reduced the expression of UBH-4::GFP mainly in the intestine, whereas undiluted *ubh-4* RNAi resulted in an almost total loss of UBH-4::GFP in all tissues (Figure 5E). Thus, experiments with diluted *ubh-4* RNAi provide an opportunity to investigate proteasome function under similar *ubh-4* expression conditions as in the long-lived *daf-2(e1370)* animals.

UBH-4 Regulates Proteasome Activity

As the long-lived *daf-2(e1370)* mutants have less UBH-4 and higher proteasome activity, we hypothesized that UBH-4 could function as a proteasome inhibitor. It has been previously shown that the human ortholog UCHL5 delays degradation of lightly polyubiquitinated substrates (Lam et al., 1997b) and that knockdown of *uchl5* in HeLa cells leads to faster degradation of the UPS reporter protein Ub-R-GFP, as well as to a reduced amount of polyubiquitinated proteins (Koulich et al., 2008). In addition, it has been reported that another proteasome-associated DUB USP14 and its yeast homolog Ubp6 attenuate proteasomal degradation (Hanna et al., 2006; Lee et al., 2010). To address if UBH-4 regulates proteasome activity in *C. elegans*, we investigated how downregulation of *ubh-4* by RNAi affected UPS activity in different tissues. Excitingly, both undiluted and diluted *ubh-4* RNAi treatment resulted in higher UPS activity in the

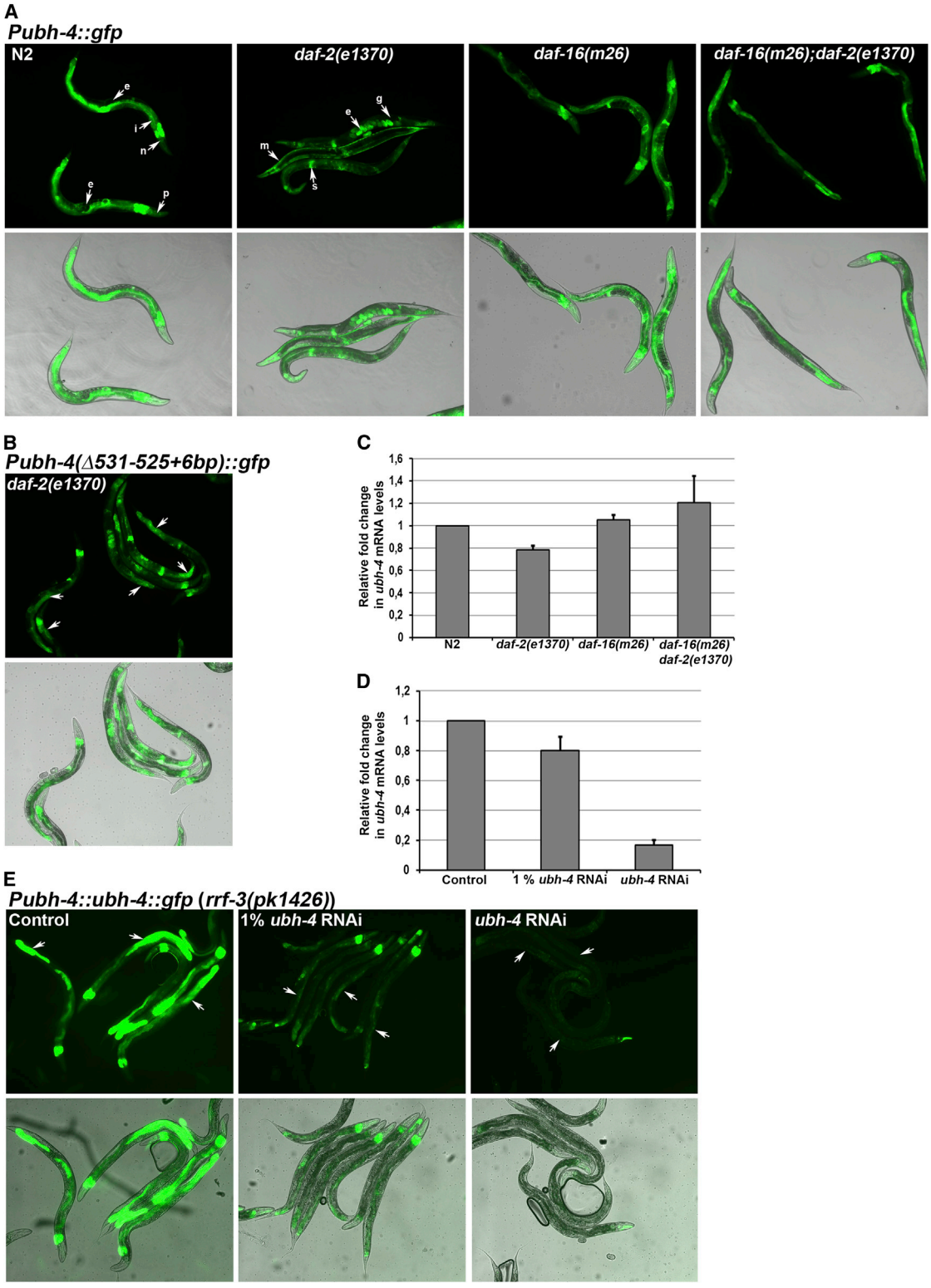

Figure 5. Expression of *ubh-4* Is Regulated in a DAF-16-Dependent Manner

(A) Expression of *Pubh-4::gfp* reporter in wild-type and IIS mutants. i, intestine; n, nerve ring; p, pharynx; g, gonad; e, embryo; m, muscle; s, spermatheca. The exposure time varies between strains.

(B) Expression of *Pubh-4(Δ531-525+6bp)::gfp* reporter in *daf-2(e1370)* animals. Arrows point intestinal expression.

(legend continued on next page)

intestine (Figures 6A and S5A). Accordingly, *ubh-4* RNAi treatments decreased the polyubiquitin reporter signal in the intestine by 0.15- to 0.18-fold (Figure 6C). The enhanced proteasome activity detected in the intestine after *ubh-4* RNAi is interesting considering that we observed accumulation of polyubiquitinated proteins in whole-animal extracts after the same treatment. This could be due to the accumulation of polyubiquitinated proteins in other tissues, because in muscle cells diluted *ubh-4* RNAi did not affect UPS activity, and undiluted *ubh-4* RNAi even caused decreased reporter degradation compared to control RNAi animals (Figures 6B and S5B). The decreased UPS activity detected in body-wall muscle cells after undiluted *ubh-4* RNAi could stem from a starting decline in general physiology, as the animals looked sick when undergoing these imaging experiments. On the whole-animal level, *ubh-4* RNAi treatments increased proteasome activity by 1.5- to 1.7-fold, as measured with proteasome in-gel activity assay in RNAi-sensitive *rrf-3(pk1426)* animals (Figures 6D and 6E). N2 animals displayed a similar trend in upregulation of proteasome activity after *ubh-4* RNAi (Figure S5C), but the effect was milder, which is probably due to the lower RNAi efficacy. The increase in proteasome activity detected in the in-gel assay after *ubh-4* knockdown did not originate from general 19S disruption, because the proteasome complexes were intact (Figure 6D) and disruption of the 19S by RPN-2 RNAi resulted in decreased proteasome activity (Figures S5D and S5E). In addition, *ubh-4* knockdown did not affect the levels of proteasome 20S alpha subunits (Figures S5F and S5G), revealing that UBH-4 directly regulates proteasome activity and not abundance.

UBH-4 Slightly Affects Lifespan and Brood Size in *C. elegans*

Because *ubh-4* knockdown resulted in enhanced proteasome activity, we investigated whether it also causes phenotypic effects such as changes in lifespan and fertility. A systematic RNAi screen previously reported that *ubh-4* RNAi slightly increases lifespan (Hamilton et al., 2005). When we performed experiments with undiluted *ubh-4* RNAi started from the L1 stage in RNAi-sensitive *rrf-3(pk1426)* animals, we did not detect an increase in lifespan, but instead consistently observed a minor decrease (Table S4). However, by using diluted *ubh-4* RNAi, a slight but significant increase in lifespan was detected (Figure 6F; Table S4). Similar to the lifespan of *rrf-3(pk1426)* animals, the lifespan of *daf-16(mgDf47);rrf-3(pk1426)* mutants was shortened by undiluted *ubh-4* RNAi, but no major changes were detected after diluted *ubh-4* RNAi treatment (Figure 6F; Table S4). The lifespan of long-lived *rrf-3(pk1426);daf-2(e1370)* mutants was not affected by either of the *ubh-4* RNAi treatments (Figure 6F; Table S4), indicating that a further decrease in the *ubh-4* mRNA level in *daf-2* mutants does not provide beneficial effects on longevity. In support of our lifespan analysis, mortality calculation revealed that diluted *ubh-4* RNAi decreased mortality of *rrf-3(pk1426)* animals (Figure 6G), but did not affect mortality of long-lived *rrf-3(pk1426);daf-2(e1370)* or short-lived *daf-16(mgDf47);rrf-3(pk1426)* mutants (Figure S6A). Knockdown of *ubh-4* by intestine- or muscle-specific *ubh-4* RNAi did not reproduce the lifespan effect in animals with normal IIS (data not shown), indicating that some additional tissue(s) including the intestine is required for the *ubh-4*-mediated lifespan extension. Importantly, ectopic expression of *ubh-4* from an intestinal promoter, which does not contain a canonical DAF-16 binding site, resulted in minor decrease in lifespan and increased mortality of *daf-2(e1370)* mutants when compared to control animals expressing intestinal Dendra2 (Figures 6H and 6I; Table S4).

We next tested whether *ubh-4* RNAi affects brood size. We detected decreased brood size in *rrf-3(pk1426)* animals after undiluted *ubh-4* RNAi (Figure S6B; Table S5), which is in line with an earlier study reporting that *ubh-4* RNAi causes embryonic lethality (Maeda et al., 2001). However, diluted *ubh-4* RNAi did not significantly decrease brood size (Figure S6B; Table S5). Brood sizes of *rrf-3(pk1426);daf-2(e1370)* or *daf-16(mgDf47);rrf-3(pk1426)* mutants were not affected by *ubh-4* RNAi treatments (Figure S6B; Table S5). Together, our data suggest that *ubh-4* is one of the many DAF-16 target genes affecting cumulatively longevity, and that there might be a threshold in the UBH-4 level for the beneficial effects on lifespan without affecting other physiological processes, such as reproduction.

ubh-4 RNAi Does Not Induce DAF-16 or SKN-1 Activation

To investigate whether the *ubh-4* RNAi-induced enhancements of proteasome activity and lifespan were derived from DAF-16-mediated effects, we measured the expression of selected DAF-16 target genes by qPCR after undiluted or diluted *ubh-4* RNAi treatments. Although we noticed some fluctuation in mRNA levels after *ubh-4* RNAi, no major changes in expression of DAF-16 target genes were observed (Figure S6C).

Next, we studied the effects of *ubh-4* RNAi on expression of SKN-1 target genes, as SKN-1, like DAF-16, is an IIS-regulated transcription factor that promotes longevity and stress responses (Tullet et al., 2008). *ubh-4* RNAi has been reported to induce SKN-1::GFP translocation into the nuclei (Kahn et al., 2008). When we performed *ubh-4* RNAi experiments, no major changes in the expression of the selected SKN-1 target genes were detected (Figure S6D). Together, our data show that the increases in longevity and proteasome activity caused by *ubh-4* knockdown do not likely originate from activation of DAF-16 or SKN-1.

Recent reports have demonstrated that increased expression of a 19S subunit encoding gene *rpn-6.1* and its human homolog *PSMD11* are required for enhanced proteasome activity in germline-deficient *C. elegans* and human embryonic stem cells, respectively (Vilchez et al., 2012a, 2012b). To test whether the

(C) Expression of *ubh-4* in wild-type and IIS mutants examined with qPCR. Graph shows the average fold changes in *ubh-4* mRNA levels compared to the wild-type (set as 1). Results are averaged from three independent experiments. Error bars, SD.
(D) Expression of *ubh-4* in *rrf-3(pk1426)* animals examined with qPCR after diluted (1%) and undiluted *ubh-4* knockdown. Graph shows the average fold changes in *ubh-4* mRNA levels compared to the control RNAi (set as 1). Results are average from four independent experiments. Error bars, SD.
(E) Expression of *Pubh-4::ubh-4::gfp* in *rrf-3(pk1426)* animals after diluted (1%) and undiluted *ubh-4* RNAi. Arrows point intestinal expression.
See also Figures S3 and S4.

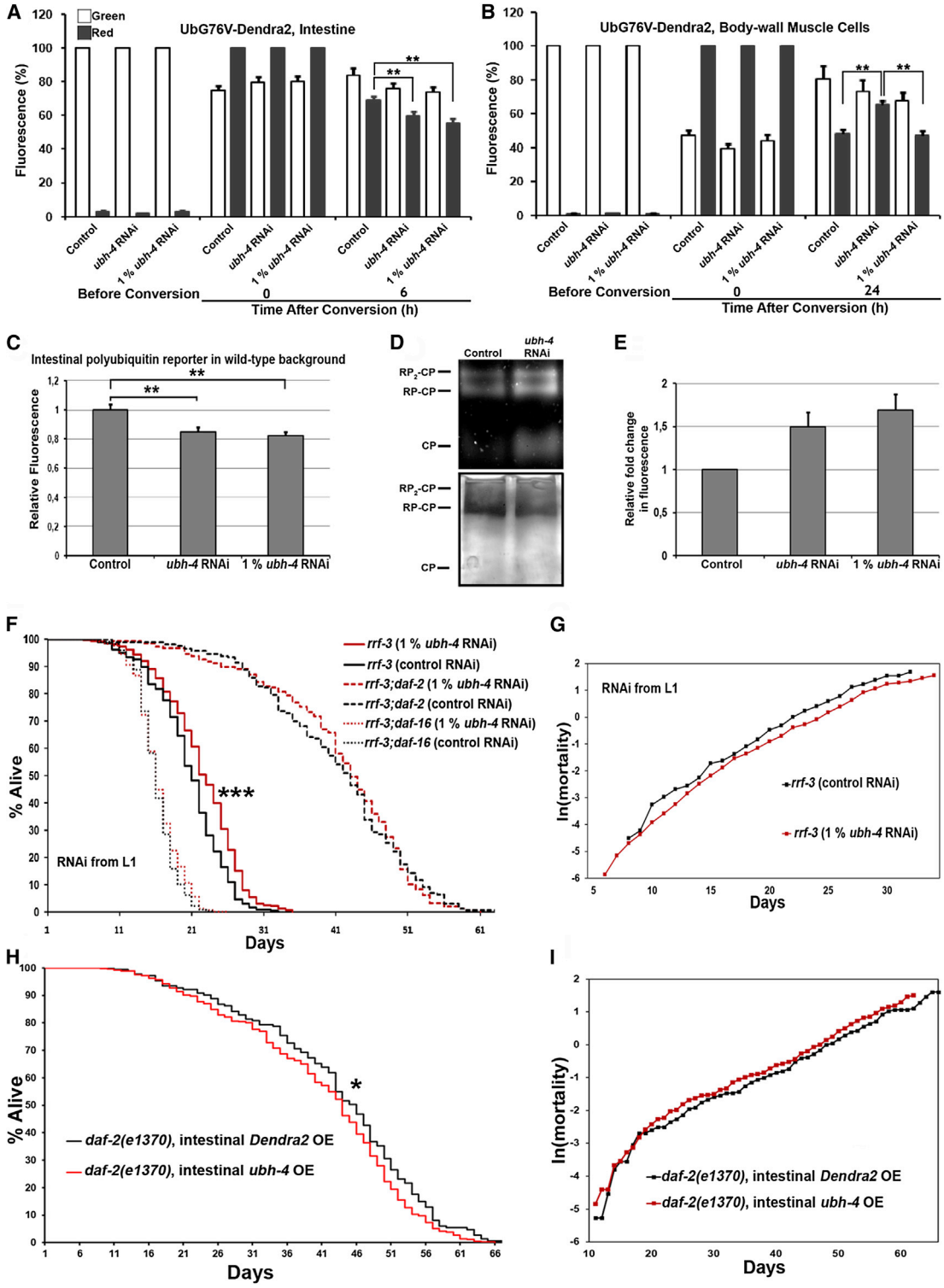

Figure 6. UBH-4 Regulates Proteasome Activity and Affects Lifespan

(A and B) (A) Quantified degradation of UbG76V-Dendra2 in intestinal cells and (B) in body-wall muscle cells of wild-type animals after control, diluted (1%), or undiluted *ubh-4* RNAi. Graphs in (A) and (B) show the average percentage of green or red fluorescence relative to the initial fluorescence intensity (before photoconversion) or the intensity at the point of photoconversion (0 hr after conversion), respectively. Error bars, SEM, $^{**}p < 0.01$, Table S2.

(C) Quantification of fluorescent intensity of intestinal polyubiquitin reporter in wild-type animals treated with control, diluted, or undiluted *ubh-4* RNAi. Graph shows average fold change in fluorescence compared to the control RNAi (set as 1). Error bars, SEM, $^{**}p < 0.01$, Table S2.

(legend continued on next page)

rpn-6.1 expression levels could be involved in the detected increases in proteasome activity reported within this study, we examined *rpn-6.1* expression in wild-type and *daf-2(e1370)* animals, as well as in *ubh-4* RNAi-treated animals. However, *daf-2(e1370)* animals and *ubh-4* RNAi-treated animals did not display an increase in *rpn-6.1* expression (Figures S6E and S6F), demonstrating that the upregulation of proteasome activity caused by reduced IIS or *ubh-4* knockdown is not mediated by changes in *rpn-6.1* expression.

uchl5 Knockdown Increases the Degradation of the Aggregation-Prone Ataxin3 Mutant

To examine if the regulation of *ubh-4* by the IIS pathway is evolutionarily conserved, we examined the expression of *uchl5* in human osteosarcoma (U-2 OS) cells under conditions of decreased IIS. By treating the cells with the PI(3)K inhibitor LY-294002, we detected approximately 30% decrease in *uchl5* mRNA levels as measured with qPCR (Figure 7A), indicating that human *uchl5* is also regulated by the IIS pathway. Next, we addressed whether UCHL5 affects proteasome activity. Knockdown of *uchl5* (Figure S7A) slightly increased degradation of UbG76V-GFP in U-2 OS cells (Figure 7B; Table S6) without decreasing the level of the control GFP (data not shown). This result is in agreement with a previous report showing that *uchl5* small interfering RNA (siRNA) increases UPS activity in HeLa cells (Koulich et al., 2008).

Previously, it has been shown that the proteasome-associated DUB USP14 prevents degradation of several proteins that cause neurotoxicity (Lee et al., 2010). We investigated if *uchl5* knockdown can also affect the levels and aggregation of the neurotoxic protein ataxin3, which is known to undergo proteasomal degradation. For this purpose, we expressed ataxin3(Q28)-GFP and ataxin3(Q84)-GFP (Chai et al., 2002) and knocked down *uchl5* in U-2 OS cells. To analyze the microscopy images of the transfected cells, we developed a method to measure cellular fluorescence intensities (representing protein levels), number of fluorescent foci (representing possible aggregates) and intensity of the foci (Figure S7B; Table S6; Experimental Procedures). *uchl5* siRNA decreased the fluorescent signal in both ataxin3(Q28)-GFP- and ataxin3(Q84)-GFP-transfected cells, indicating that degradation of the transfected proteins was increased (Figure 7C; Table S6). We also detected a slight decrease in the number and a clear decrease in the intensity of the fluorescent foci in ataxin3-GFP-transfected cells after *uchl5* siRNA (Figure S7C; Table S6), implying that decreased levels of the transfected proteins affect the formation of aggregates. Together, these results show that, similar to the IIS-regulated UBH-4 in *C. elegans* (Figure 7D), a decreased level of UCHL5 increases UPS activity and enhances degradation of aggregation prone proteins in human cells.

DISCUSSION

The data we present establish an in vivo mechanism by which IIS regulates proteasome activity through the FOXO transcription factor DAF-16 target *ubh-4*. Together with Dr. Blackwell's group, we have previously shown that the IIS is involved in regulating proteasome activity through the transcription factor SKN-1 in *C. elegans* (Li et al., 2011). Studies by other groups have also reported links between UPS and IIS by showing that FOXO transcription factors regulate the expression of ubiquitin ligases MAFbx and MuRF1, which contribute to muscle atrophy (Sandri et al., 2004; Stitt et al., 2004). Recent studies have also highlighted the roles of DAF-16 and FOXO4 in regulation of proteasome activity in germline-lacking *C. elegans* and human embryonic stem cells, respectively (Vilchez et al., 2012a, 2012b). In addition, DAF-16 and possibly some other IIS components are under proteasomal control, which affects lifespan in *C. elegans* (Kuhlbrodt et al., 2011; Li et al., 2007). Here, we have identified the DUB *ubh-4* as differentially expressed in wild-type and long-lived *daf-2* IIS mutants.

The increase in UbG76V-Dendra2 degradation and decrease in accumulation of polyubiquitinated proteins in the intestine, which we observed upon *ubh-4* RNAi, may stem from reduced ubiquitin chain trimming by UBH-4. In accordance, previous studies have demonstrated that proteasomal degradation of ubiquitinated substrates can be enhanced by deleting or inhibiting the ubiquitin-chain-trimming DUBs UCHL5 (UBH-4 ortholog) or USP14 (Koulich et al., 2008; Lam et al., 1997a, 1997b; Lee et al., 2010). It is likely that UBH-4 also regulates proteasome activity in a noncatalytic manner, perhaps by inhibiting substrate entry to the proteolytic core, as we observed that *ubh-4* knockdown increases proteasome activity also in the ubiquitination independent in-gel activity assay. Interestingly, the yeast homolog of USP14, Ubp6, has been shown to inhibit substrate degradation in a manner independent of its deubiquitinating activity (Hanna et al., 2006). On the other hand, binding of polyubiquitinated proteins to USP-14 and UCHL5 can also activate proteasomal ATPases (Peth et al., 2013). Thus, proteasome-associated DUBs appear to exert their regulatory effects through multiple mechanisms.

(D) Lysates of *rrf-3(pk1426)* animals treated with control or *ubh-4* RNAi separated on a native gel followed by in-gel proteasome activity assay with fluorogenic suc-LLVY-AMC substrate. Lower panel shows Coomassie staining of the gel.
(E) Quantification of proteasome in-gel activity from *rrf-3(pk1426)* animals treated with control, diluted or undiluted *ubh-4* RNAi. Graph shows the average fold change compared to the control RNAi (set as 1). Results are mean of quantifications (control and *ubh-4* RNAi n = 15, diluted *ubh-4* RNAi n = 10 independent experiments). Error bars, SEM.
(F) Kaplan-Meier survival analysis of *rrf-3(pk1426)*, *rrf-3(pk1426);daf-2(e1370)* and *daf-16(mgDf47);rrf-3(pk1426)* animals treated with control or diluted (1%) *ubh-4* RNAi started from the L1 stage (log-rank test, ***$p < 0.0001$, Table S4).
(G) Mortality of *rrf-3(pk1426)* animals treated with control or diluted (1%) *ubh-4* RNAi. Data used for analysis are the same as in (F).
(H) Kaplan-Meier survival analysis of *daf-2(e1370)* mutants with intestinal *ubh-4* overexpression (*ubh-4* OE) (log-rank test, *$p < 0.05$, Table S4).
(I) Mortality of *daf-2(e1370)* mutants with intestinal *ubh-4* overexpression (*ubh-4* OE) and control animals expressing intestinal Dendra2. Data used for analysis are the same as in (H), Table S4.
See also Figure S6.

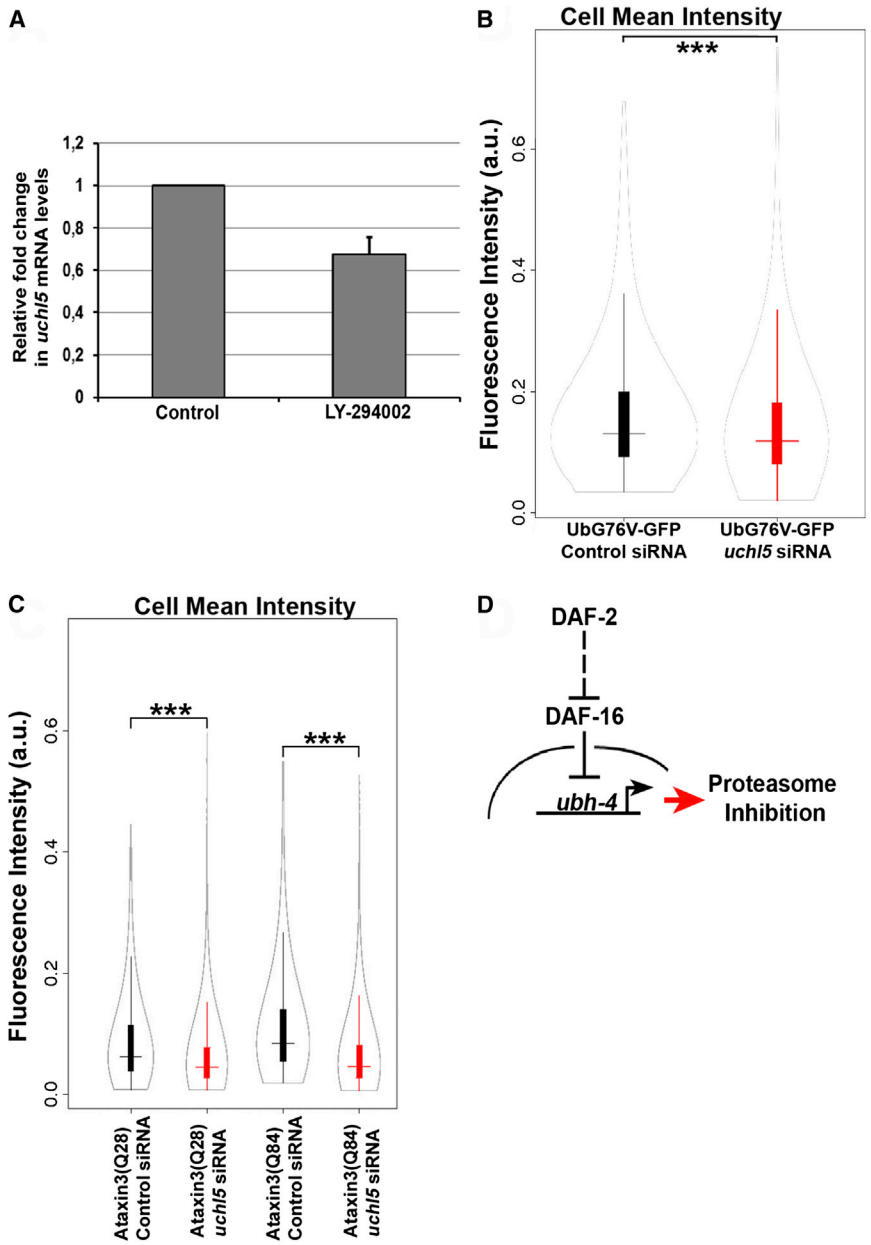

Figure 7. *uchl5* siRNA Increases UPS Activity and Degradation of Proteins Linked to Proteotoxicity in Human Cells

(A) Expression of *uchl5* in U-2 OS cells after PI(3)K inhibitor LY-294002 treatment (20 μM, 7 hr) examined with qPCR. Graph shows the average fold change in *uchl5* mRNA levels compared to the DMSO-treated control (set as 1). Results are average from three independent experiments. Error bar, SD.

(B) Violin plots showing mean cell fluorescence intensity in U-2 OS cells transfected with vector encoding UbG76V-GFP and control or *uchl5* siRNA and (C) with vectors encoding ataxin3(Q28)-GFP or ataxin3(Q84)-GFP and control or *uchl5* siRNA (***$p < 0.001$, Table S6).

(D) A model for IIS-regulated proteasome activity. Decreased IIS mediated by *daf-2* mutation activates DAF-16 resulting in downregulation of *ubh-4* expression, which, in turn, upregulates proteasome activity.

See also Figure S7.

Surprisingly, we detected increased accumulation of polyubiquitinated proteins in whole-animal extracts after *ubh-4* RNAi, although proteasome activity increased according to the in-gel proteasome activity assay and the intestinal fluorescent reporters. This could be a consequence of proteasome inhibition in other tissues, such as body-wall muscle, in which we detected decreased proteasome activity after *ubh-4* RNAi. The tissue-specific effects of *ubh-4* knockdown could derive from variable expression levels of *ubh-4* between tissues, but also from differential expression of, for example, the proteasomal polyubiquitin receptor *rpn-13.* In mammalian cells, association of UCHL5 with RPN13 has been reported to activate UCHL5 (Yao et al., 2006). Alternatively, UBH-4 might possess the same function as UCHL5 in rescuing poorly ubiquitinated substrates from degradation (Lam et al., 1997b). In this scenario, deubiquitination leads to substrate dissociation from the proteasome. Therefore, in our case, knockdown of ubiquitin-chain-trimming UBH-4 may lead to preferred and faster degradation of lightly ubiquitinated substrates and to the accumulation of heavily polyubiquitinated proteins, which can then be detected in the polyubiquitin western blot.

We have previously shown that the IIS-regulated SKN-1 affects proteasome activity mainly in the intestine (Li et al., 2011). The role of DAF-16 as a proteasome activity modulator through UBH-4 is also most prominent in the intestine, where *ubh-4* expression is downregulated in a DAF-16-dependent manner. Recent reports suggest a high degree of complexity in regulation of DAF-16-mediated processes with different isoforms crosstalking, regulating partly distinct sets of genes, and showing tissue specificity (Kwon et al., 2010). Additionally, the growth factor IGF-1, which inhibits FOXO activity, increases proteasome activity in mouse brain frontal cortex lysates (Crowe et al., 2009), whereas overexpression of constitutively active FOXO3 slightly increases proteasomal degradation in myotubes (Zhao et al., 2007). Together with these reports, our results establish that proteasome activity is under cell-type-specific regulation by the IIS.

Enhancement of proteasome activity has been shown to extend lifespan in yeast and *Drosophila* (Kruegel et al., 2011; Tonoki et al., 2009), and high proteasome activity has been observed in lysates from long-lived naked mole-rats and

fibroblasts derived from centenarians (Chondrogianni et al., 2000; Pérez et al., 2009). Additionally, a recent study reported that ectopic expression of *rpn-6* in *C. elegans* resulted in upregulated proteasome activity and extended lifespan during mild heat stress (Vilchez et al., 2012b). We suggest that the mild effect of UBH-4 on *C. elegans* lifespan could derive from its regulation of proteasome activity. The minor lifespan effect of *ubh-4* downregulation is in agreement with the cooperative action of the DAF-16 target genes on longevity (Kenyon, 2010). Because both activation of the proteasome and the slight increase in lifespan are attained after an approximate 20% decrease in total *ubh-4* mRNA, we speculate that a subpopulation of proteasome complexes is lacking the associated UBH-4. Under these conditions, the proteasome-associated deubiquitinating activity would not be downregulated to an extent causing negative physiological effects, emphasizing the fine balance in gene expression required to control cellular processes.

In addition to our results showing that the IIS/DAF-16 pathway regulates proteasome activity, epidermal growth factor signaling has been reported to affect proteasomal degradation and longevity (Liu et al., 2011). Modulation of proteasome activity through multiple lifespan regulating pathways would provide flexibility in meeting the proteostasis requirements upon aging. Similar to many of the cellular processes in metazoans, we show that the enhancement of proteasome activity through downregulation of *ubh-4* is evolutionarily conserved. Affecting the IIS in a cell-type-specific manner could create opportunities to modulate the proteasome in age-related disorders exhibiting dysfunctional proteasome.

EXPERIMENTAL PROCEDURES

Nematodes

C. elegans strains were grown under standard conditions (Brenner, 1974) at 20°C. N2 (Bristol) strain was used as the wild-type. N2, CB1370: *daf-2(e1370)III*, DR26: *daf-16(m26)I*, GR1307: *daf-16(mgDf50)I*, DR1309: *daf-16(m26)I;daf-2(e1370)II*, GR1309: *daf-16(mgDf47)I;daf-2(e1370)III*, CF1814: *rrf-3(pk1426)II;daf-2(e1370)III*, IU10: *daf-16(mgDf47)I;rrf-3(pk1426)II*, NR350: *rde-1(ne219)V;kzIs20*, and VP303: *rde-1(ne213)V;kbIs7* were obtained from the Caenorhabditis Genetics Center (CGC). NL2099: *rrf-3(pk1426)II* mutant strain was a generous gift from Dr. G. Wong (University of Eastern Finland). Transgenic lines used in this study are listed in Table S1.

Lifespan Assays and Progeny Counts

All lifespan experiments were performed at 20°C. Synchronized animals were plated on RNAi feeding plates as L1 larvae (day 1). Animals were transferred to a new plate every second day and, once they stopped producing offspring, every few days. Animals were checked every day and classified as dead when they failed to respond to a gentle prod with a platinum pick. Animals that crawled off the plate, died from an extruded gonad or had internally hatched offspring were censored at the time of their death. Each survival assay was repeated two to five times. For progeny counts, synchronized animals were plated on RNAi feeding plates as L1 larvae. Animals were moved to fresh RNAi plates every day until they stopped producing offspring. Total viable offspring per animal was counted. The offspring of animals that crawled off the plate died of internally hatched offspring or an extruded gonad before having stopped laying eggs were censored. Experiments were repeated three to five times.

Plasmids and Generation of Transgenic Lines

Cloning of *Dendra2* and *UbG76V-Dendra2* expression vectors has been described earlier (Hamer et al., 2010; Li et al., 2011). *pPubh-4::gfp* expression vector was created by amplifying 1375 bp promoter region upstream and 264 bp downstream of the *ubh-4* coding region using PCR (see Table S7 for all primers used for cloning in this study). The PCR product amplified upstream of *ubh-4* coding region was digested with PciI and AgeI, and the downstream amplified PCR product was digested with NotI. Sequences were cloned into the *pPD30.38* expression vector containing GFP coding sequence cloned between inserted AgeI and NotI restriction sites (the *unc-54* promoter and enhancer were replaced).

To create the *pPubh-4(D531-525+6bp)::gfp* expression vector, the *pPubh-4::gfp* expression vector was amplified with PCR using oligonucleotides having SmaI restriction site in place of DAF-16 consensus sequence (gtaaaca). To create the *pPubh-4::ubh-4::gfp* expression vector, the *ubh-4* coding region amplified with PCR from *C. elegans* cDNA was digested with AgeI and cloned into the *pPubh-4::gfp* expression vector.

To create *pPubh-4::His-gfp* expression vector, the sequence encoding His-SBP tag was amplified with PCR (from Gateway *Drosophila* expression vector, kind gift of Dr. Jussi Taipale), digested with AgeI, and inserted in front of the GFP sequence in *pPubh-4::gfp* expression vector. For *pPubh-4::His-ubh-4-gfp* expression vector, GFP was replaced between NheI and AgeI sites with *ubh-4* coding region amplified with PCR from *C. elegans* cDNA. Expression vector *pPrpn-13::HA-RPN-13* was created by amplifying with PCR 1,100 bp promoter sequence upstream of *rpn-13* coding region. The PCR product was digested with EcoRV and AgeI and ligated into PciI (blunted with Klenow fragment) and AgeI-digested *pPubh-4::gfp* expression vector to replace *ubh-4* promoter. GFP was replaced with *rpn-13* coding region, which was amplified with PCR from *C. elegans* cDNA. PCR product was digested with AgeI and Acc65I. The sequence encoding HA tag was amplified with PCR (from Gateway *Drosophila* expression vector, kind gift of Dr. Jussi Taipale), and the product was digested with AgeI and ligated in front of the *rpn-13* coding sequence. To create vector for intestinal *ubh-4* overexpression (*pPvha-6::ubh-4*), the *ubh-4* coding region, amplified with PCR from *C. elegans* cDNA (digested with AgeI and NheI and blunted with Klenow fragment), was used to replace the *ZsGreen* coding sequence in NheI- and NotI-digested, Klenow-fragment-blunted *pPvha-6::ZsGreen* expression vector (not used in this study). All transgenic lines were created by microinjection (Mello et al., 1991). Of the strains carrying extrachromosomal arrays, four independent lines expressing transcriptional- or translational *ubh-4* reporters, two independent lines of *Dendra2* or *UbG76V-Dendra2* transgenic strains, and one line of both strains used in immunoprecipitation experiments were isolated and analyzed. Results shown are representative of all lines.

To create *ZsProSensor* expression vector for intestinal cells, *ZsProSensor* coding sequence was cut from *pZsProSensor-1* vector (Clontech) with NheI and NotI and ligated into the NheI- and NotI-digested *pPD30.38* expression vector (Addgene, Fire Lab vector kit) containing *unc-54* promoter. To create polyubiquitin reporter (*UIM2-ZsProSensor*) expression constructs for intestinal cells, *ZsGreen-MODC* coding sequence was amplified with PCR from *pZsProSensor-1* vector (Clontech). PCR product was digested with AgeI and NotI. Coding sequence for polyubiquitin binding motifs (UIMs, amino acids 195–313) of the RPN-10 was amplified with PCR from *C. elegans* cDNA, and the product was digested with NheI and AgeI. PCR fragments were ligated into the NheI- and NotI-digested *pPD30.38* expression vector containing *unc-54* promoter. The *vha-6* promoter was amplified with PCR from *Pvha-6::HSF-1* expression vector (Morley and Morimoto, 2004) (kind gift of Dr. Richard Morimoto). The PCR product was digested with PciI and NheI and used to replace *unc-54* promoter in both *ZsProSensor* and polyubiquitin reporter expression vectors. The Polyubiquitin reporter extrachromosomal array was integrated using gamma irradiation and backcrossed five times with wild-type. One line carrying integrated transgene was used in experiments. The integrated line carrying polyubiquitin reporter transgene in *daf-2(e1370)* background was created by crossing.

For mammalian cell culture experiments, expression vectors *pEGFP-C1-Ataxin3Q28* (Addgene plasmid 22122), *pEGFP-C1-Ataxin3Q84* (Addgene plasmid 22123) (Chai et al., 2002), and *UbG76V-GFP* (Addgene plasmid 11941) (Dantuma et al., 2000) were purchased from Addgene. *pEGFP-C2* expression vector (kind gift of Dr. Marikki Laiho) was used to express GFP in mammalian cells.

Mammalian Cell Culturing

Human osteosarcoma (U-2 OS) cells were cultured in Dulbecco's modified Eagle's medium with 15% fetal bovine serum (GIBCO). For siRNA experiments, FlexiTube GeneSolution for *uchl5* (QIAGEN) and AllStars Negative Control siRNA (QIAGEN) were used with HiPerFect Transfection Reagent (QIAGEN). Cells were incubated for 3 days with medium containing siRNAs. Expression vectors for *ataxin3(Q28)*, *ataxin3(Q84)*, and *UbG76V-GFP* were transfected with Fugene 6 (Roche) a day after siRNA transfection. Cells were fixed with 3.5% paraformaldehyde in PBS. For PI(3)K inhibition, U-2 OS cells were incubated for 7 hr with 20 μM LY-294002 (Enzo Life Sciences).

C. elegans RNA Interference

Unless otherwise indicated, RNAi was performed using the feeding protocol as described earlier (Timmons et al., 2001). *E. coli* strain HT115 carrying the empty *pL4440* expression vector was used as a control in experiments with RNAi clones from J. Ahringer library. *daf-2(e1370)* mutants carrying intestinal UbG76V-Dendra2 were placed on *rpn-2* RNAi (C23G10.4, J. Ahringer library) as L3 larvae 2 days before photoconversion. For proteasome in-gel activity assays, *rrf-3(pk1426)* animals were placed on *rpn-2* RNAi as L4 larvae and harvested 2 days later. Animals expressing polyubiquitin reporter in the intestine were maintained on control RNAi bacteria and transferred to *rpn-2* RNAi at L4 larvae and imaged 3 days later. Bacteria carrying empty RNAi vector (*pL4440*) was used to dilute *ubh-4* RNAi bacteria. In imaging experiments, *ubh-4* and *lgg-1* (*C08B11.7* and *C32D5.9*, respectively, J. Ahringer library) RNAi were initiated from hatching. *ubh-4* RNAi was initiated from L1 stage in proteasome in-gel activity assays, lifespan experiments, and progeny counts. For *daf-16* RNAi (*pAD43*) and *pAD12* (control RNAi for *daf-16*) (kind gifts of Dr. Andrew Dillin), 10 mM isopropyl β-D-1-thiogalactopyranoside (IPTG) was used to induce production of double-stranded RNA, and, before seeding the plates, IPTG concentration was added to 20 mM. *L4440-daf-16a* (Addgene plasmid 31503) and *L4440-daf-16 df* (Addgene plasmid 31505) RNAi expression vectors (Kwon et al., 2010) were purchased from Addgene. *daf-16* RNAi was initiated from hatching in all experiments and imaged at first day of adulthood.

C. elegans Immunofluorescence

An unsynchronized population of animals expressing polyubiquitin reporter was fixed and permeabilized as described previously (Finney and Ruvkun, 1990). Polyubiquitinated proteins were immunostained with FK1 antibody (Enzo) and visualized with Alexa Fluor 594 (Invitrogen).

Microscopy, Image Analysis, Equipment, and Settings

For UbG76V-Dendra2 and Dendra2 imaging, young adult (4 and 5 days old with transgenic animals in *daf-2(e1370)* background) animals were imaged. Dendra2 imaging was done as described earlier (Hamer et al., 2010). Briefly, animals were mounted on an agarose pad on glass slides and immobilized using 0.5 mM levamisole in M9 (22 mM KH_2PO_4, 41 mM Na_2HPO_4, 8.5 mM NaCl, and 19 mM NH_4Cl). Animals were recovered on feeding plates in between imaging steps. For confocal imaging, a motorized Zeiss Axio Observer Z1 inverted microscope with LSM 5 Live line scanner and LSM AIM software Rel. 4.2 was used. Images were acquired with 63 × 1.4 numerical aperture (NA) plan-apochromat objective. Photoconversion was carried out using a diode 405 nm (50 mW). Diode-pumped solid-state (DPSS) (488 nm; 100 mW) and 561 nm DPSS (40 mW) lasers were used to visualize Dendra2 before and after photoconversion. To facilitate image analysis, gain/laser power of the red channel was adjusted to get approximately similar red fluorescence intensity in each sample after photoconversion. Images were acquired at a depth of 8 bits per channel and 512 × 512 pixels (scanning speed 177.62 μs per pixel) at a pixel resolution of 210 nm. Fluorescence intensities were analyzed with Zeiss LSM Image Examiner version 4.2. To calculate the relative intensities, the absolute values of fluorescence before and right after photoconversion were set as 100% for the green and red fluorescence signals, respectively. Fluorescence images are pseudocolored using Zeiss LSM Image Examiner version 4.2.

Polyubiquitin reporter animals treated with *ubh-4* or *rpn-2* RNAi were imaged at 6 days old or as young adults (4 and 5 days old with transgenic animals in *daf-2[e1370]* background) after *daf-16* RNAi. Animals carrying *Pubh-4::gfp* or *Pubh-4(Δ531-525+6bp)::gfp* transcriptional or *Pubh-4::ubh-4::gfp* translational reporter were imaged as young adults (4 and 5 days old with transgenic animals in *daf-2(e1370)* background). Polyubiquitin reporter, *Pubh-4::gfp*, and *Pubh-4(Δ531-525+6bp)::gfp* transcriptional and *Pubh-4::ubh-4::gfp* translational reporter animals were imaged with a Zeiss Axioplan 2 microscope using 10× 0.3 NA objective. Fluorescence signal intensity from the intestine of polyubiquitin reporter animals was quantified with Fiji. Confocal images of the FK1 immunostained polyubiquitin reporter animals were taken by using a motorized Zeiss AxioVert 200 M inverted microscope with LSM 510 point scanner and LSM software release 3.2. Images were acquired with 63 × 1.4 NA plan-apochromat objective, and 488 nm argon (30 mW) and 543 nm helium-neon (1 mW) lasers.

U-2 OS cells transfected with *uchl5* siRNA and constructs expressing GFP and wild-type or mutant ataxin3 were imaged with Zeiss Axioplan 2 microscope using 20 × 0.5 NA objective. Analysis of fluorescence intensities and aggregate counts (with ataxin3) were made in a computational pipeline created in the freely available Anduril analysis framework (Ovaska et al., 2010). The pipeline begins with finding the cytoplasm based on the GFP channel. To aid the segmentation, nuclei from Hoechst channel were also detected. The cell fluorescence intensity measurements were done based on the cytoplasm segmentation. Local maxima with radii of three and seven pixels were detected in the GFP channel and joined together and grown to three pixel radius disks. These points represent the aggregates in the signal, and thus the aggregate-related measurements were done on the disk areas. U-2 OS cells transfected with *uchl5* siRNA and *UbG76V-GFP* were imaged with Zeiss Axioplan 2 microscope using 10 × 0.3 NA objective. The cell fluorescence intensity measurements were done as described above.

Quantitative Real-Time PCR

For RNA extraction from each strain or RNAi experiment, synchronized young adult animals (4 and 5 days old with *daf-2[e1370]* strain) were harvested. Total RNA was extracted using a NucleoSpin RNA II kit (Macherey-Nagel) or GeneJet RNA Purification Kit (Fermentas). RT-PCR was done using a Maxima First Strand cDNA Synthesis Kit for RT-qPCR (Fermentas). Quantitative real-time PCR was done using Maxima SYBR Green/ROX qPCR Master Mix (2×) (Fermentas) and LightCycler 480 (Roche) quantitative PCR machine. *ubh-4* and *rpn-6.1* qPCR data were normalized to the geometric mean of three reference gene mRNA concentrations (*act-1*, *cdc-42*, and *pmp-3*) (Vandesompele et al., 2002). DAF-16 and SKN-1 target gene qPCR data were normalized with *act-1* mRNA concentrations, and qPCR data from mammalian cells were normalized with *gapdh* mRNA concentrations. For qPCR oligonucleotide sequences, see Table S7.

Native Gel Electrophoresis

Age-synchronized young adult animals (4 and 5 days old with *daf-2[e1370]* strain) were collected to M9 prior to freezing in –80°C. Animals were lysed using Dounce homogenizer and native gel lysis buffer (Elsasser et al., 2005). Native gel electrophoresis and developing of the gel was performed like reported earlier (Elsasser et al., 2005) with minor modifications. Gels were run in ice bath for 3 or 6 hr using 40 or 20 mA as a constant, respectively. Developing buffer with 80 μM of suc-LLVY-AMC (Bachem) was used to develop the gel. Coomassie staining was done with Colloidal Blue Staining Kit (Invitrogen). For deubiquitinating assay on native gel, electrophoresis was done like described above. Development of the gel was done in developing buffer (Elsasser et al., 2005) supplied with 1 mM Ub-AMC (Boston Biochem) for 1 hr at 30°C. Gels were imaged with MultiImage Light Cabinet using FluorChem (3.04B) program (Alpha Innotech Corporation). Signal levels were adjusted using Photoshop 9.0 (Adobe Systems) and quantified analyzed using Fiji. The quantification of the proteasome activity is the sum of fluorescent signal within the bands representing RP_2-CP, RP-CP, and CP. As a technical point, we noticed that the proteasome activity measurements using the in-gel activity assay produce sometimes inconsistent results, and therefore multiple repeats were performed.

Mass Spectrometry Analysis

The proteins were separated using native gel and visualized with Coomassie staining. For protein identification, gel lanes containing RP_2-CP and RP-CP proteasome complexes were extracted followed by in-gel trypsin digestion.

Peptides were analyzed by liquid chromatography tandem mass spectrometry (LC-MS/MS) using an Ultimate 3000 nano-LC (Dionex) and a QSTAR Elite hybrid quadrupole TOF-MS (Applied Biosystems/MDS Sciex) with nano-ESI ionization as described previously (Ohman et al., 2010). The LC-MS/MS data were searched with in-house Mascot version 2.2 through ProteinPilot 3.0 interface against the NCBInr 20100513 database (10,987,230 sequences; 3,739,173,051 residues, taxonomy: *C. elegans* [28,762 sequences]). All of the reported protein identifications are statistically significant ($p < 0.05$).

Immunoprecipitation and Western Blotting

His-tag immunoprecipitation was done with Protino Ni-NTA agarose (Macherey-Nagel). Western blot samples were separated on a polyacrylamide gel and blotted onto a nitrocellulose membrane using a semidry blotting system (Bio-Rad). FK1 antibody for polyubiquitinated proteins (Enzoproteasome 20S α1, 2, 3, 5, 6, and 7 subunits antibody (Enzo), anti-α-tubulin antibody (Sigma), streptavidin-HRP (Dako), and anti-HA antibody (Covance) were used in blotting. Signal levels were adjusted using Photoshop 9.0 (Adobe Systems) and quantified using Fiji.

Statistical Analysis

With Dendra2 and polyubiquitin reporter imaging, the statistical difference of relative protein degradation between different strains or RNAi treatments was determined by applying the Student's t test (two-tailed). Lifespan statistics were performed on R, with Kaplan-Meier survival plot and stratified log-rank test (Mantel-Cox). Mortality was calculated by using ln $[-\ln(p_x)]$ formula (where p_x is survival probability at day x to x + 1). With progeny counts, the statistical difference between different RNAi treatments was determined by applying the Student's t test (two-tailed). Statistical analysis of mammalian cell image data was performed by applying Student's t test (two-tailed).

SUPPLEMENTAL INFORMATION

Supplemental Information includes seven figures and seven tables and can be found with this article online at http://dx.doi.org/10.1016/j.celrep.2013.05.012.

LICENSING INFORMATION

ACKNOWLEDGMENTS

This work was supported by grants from the Academy of Finland (nos. 131408 and 259797 to C.I.H. and no. 125826 to S.H.) and by grants to CIH from the International Human Frontier Science Program Organization, the Sigrid Jusélius Foundation, the Magnus Ehrnrooth Foundation, Medicinska understödsföreningen Liv och Hälsa r.f., Biocentrum Helsinki, and University of Helsinki. O.M. and L.A. were supported by the Helsinki Biomedical Graduate Program (HBGP). The authors thank Drs. Marikki Laiho, Jussi Taipale, Richard Morimoto, Andrew Dillin, and Garry Wong for sharing reagents, plasmids, RNAi clones, and *C. elegans* strains, the Biomedicum Imaging Unit (BIU) for their help with imaging, the Protein Chemistry Research Group and Core Facility (University of Helsinki) for mass spectrometry analysis, and Anni-Helena Sukupolvi and Elisa Mikkonen for assistance with the experiments. We thank Caenorhabditis Genetics Center (funded by the National Institutes of Health - National Center for Research Resources) for providing *C. elegans* strains.

Received: June 7, 2012
Revised: April 15, 2013
Accepted: May 8, 2013
Published: June 13, 2013

REFERENCES

Balch, W.E., Morimoto, R.I., Dillin, A., and Kelly, J.W. (2008). Adapting proteostasis for disease intervention. Science *319*, 916–919.

Ben-Zvi, A., Miller, E.A., and Morimoto, R.I. (2009). Collapse of proteostasis represents an early molecular event in Caenorhabditis elegans aging. Proc. Natl. Acad. Sci. USA *106*, 14914–14919.

Bennett, E.J., Shaler, T.A., Woodman, B., Ryu, K.Y., Zaitseva, T.S., Becker, C.H., Bates, G.P., Schulman, H., and Kopito, R.R. (2007). Global changes to the ubiquitin system in Huntington's disease. Nature *448*, 704–708.

Brenner, S. (1974). The genetics of Caenorhabditis elegans. Genetics *77*, 71–94.

Celniker, S.E., Dillon, L.A., Gerstein, M.B., Gunsalus, K.C., Henikoff, S., Karpen, G.H., Kellis, M., Lai, E.C., Lieb, J.D., MacAlpine, D.M., et al.; modENCODE Consortium. (2009). Unlocking the secrets of the genome. Nature *459*, 927–930.

Chai, Y., Shao, J., Miller, V.M., Williams, A., and Paulson, H.L. (2002). Live-cell imaging reveals divergent intracellular dynamics of polyglutamine disease proteins and supports a sequestration model of pathogenesis. Proc. Natl. Acad. Sci. USA *99*, 9310–9315.

Chondrogianni, N., Petropoulos, I., Franceschi, C., Friguet, B., and Gonos, E.S. (2000). Fibroblast cultures from healthy centenarians have an active proteasome. Exp. Gerontol. *35*, 721–728.

Cohen, E., Bieschke, J., Perciavalle, R.M., Kelly, J.W., and Dillin, A. (2006). Opposing activities protect against age-onset proteotoxicity. Science *313*, 1604–1610.

Cohen, E., Paulsson, J.F., Blinder, P., Burstyn-Cohen, T., Du, D., Estepa, G., Adame, A., Pham, H.M., Holzenberger, M., Kelly, J.W., et al. (2009). Reduced IGF-1 signaling delays age-associated proteotoxicity in mice. Cell *139*, 1157–1169.

Crowe, E., Sell, C., Thomas, J.D., Johannes, G.J., and Torres, C. (2009). Activation of proteasome by insulin-like growth factor-I may enhance clearance of oxidized proteins in the brain. Mech. Ageing Dev. *130*, 793–800.

Dahlmann, B. (2007). Role of proteasomes in disease. BMC Biochem. *8*(*Suppl 1*), S3.

Dantuma, N.P., Lindsten, K., Glas, R., Jellne, M., and Masucci, M.G. (2000). Short-lived green fluorescent proteins for quantifying ubiquitin/proteasome-dependent proteolysis in living cells. Nat. Biotechnol. *18*, 538–543.

David, D.C., Ollikainen, N., Trinidad, J.C., Cary, M.P., Burlingame, A.L., and Kenyon, C. (2010). Widespread protein aggregation as an inherent part of aging in C. elegans. PLoS Biol. *8*, e1000450.

Dong, M.Q., Venable, J.D., Au, N., Xu, T., Park, S.K., Cociorva, D., Johnson, J.R., Dillin, A., and Yates, J.R., 3rd. (2007). Quantitative mass spectrometry identifies insulin signaling targets in C. elegans. Science *317*, 660–663.

Elsasser, S., Schmidt, M., and Finley, D. (2005). Characterization of the proteasome using native gel electrophoresis. Methods Enzymol. *398*, 353–363.

Finley, D. (2009). Recognition and processing of ubiquitin-protein conjugates by the proteasome. Annu. Rev. Biochem. *78*, 477–513.

Finney, M., and Ruvkun, G. (1990). The unc-86 gene product couples cell lineage and cell identity in C. elegans. Cell *63*, 895–905.

Furuyama, T., Nakazawa, T., Nakano, I., and Mori, N. (2000). Identification of the differential distribution patterns of mRNAs and consensus binding sequences for mouse DAF-16 homologues. Biochem. J. *349*, 629–634.

Hamazaki, J., Iemura, S., Natsume, T., Yashiroda, H., Tanaka, K., and Murata, S. (2006). A novel proteasome interacting protein recruits the deubiquitinating enzyme UCH37 to 26S proteasomes. EMBO J. *25*, 4524–4536.

Hamer, G., Matilainen, O., and Holmberg, C.I. (2010). A photoconvertible reporter of the ubiquitin-proteasome system in vivo. Nat. Methods *7*, 473–478.

Hamilton, B., Dong, Y., Shindo, M., Liu, W., Odell, I., Ruvkun, G., and Lee, S.S. (2005). A systematic RNAi screen for longevity genes in C. elegans. Genes Dev. *19*, 1544–1555.

Hanna, J., and Finley, D. (2007). A proteasome for all occasions. FEBS Lett. *581*, 2854–2861.

Hanna, J., Hathaway, N.A., Tone, Y., Crosas, B., Elsasser, S., Kirkpatrick, D.S., Leggett, D.S., Gygi, S.P., King, R.W., and Finley, D. (2006). Deubiquitinating enzyme Ubp6 functions noncatalytically to delay proteasomal degradation. Cell *127*, 99–111.

Hershko, A., and Ciechanover, A. (1998). The ubiquitin system. Annu. Rev. Biochem. *67*, 425–479.

Hsu, A.L., Murphy, C.T., and Kenyon, C. (2003). Regulation of aging and age-related disease by DAF-16 and heat-shock factor. Science *300*, 1142–1145.

Kahn, N.W., Rea, S.L., Moyle, S., Kell, A., and Johnson, T.E. (2008). Proteasomal dysfunction activates the transcription factor SKN-1 and produces a selective oxidative-stress response in Caenorhabditis elegans. Biochem. J. *409*, 205–213.

Kenyon, C. (2005). The plasticity of aging: insights from long-lived mutants. Cell *120*, 449–460.

Kenyon, C.J. (2010). The genetics of ageing. Nature *464*, 504–512.

Kenyon, C., Chang, J., Gensch, E., Rudner, A., and Tabtiang, R. (1993). A C. elegans mutant that lives twice as long as wild type. Nature *366*, 461–464.

Koulich, E., Li, X., and DeMartino, G.N. (2008). Relative structural and functional roles of multiple deubiquitylating proteins associated with mammalian 26S proteasome. Mol. Biol. Cell *19*, 1072–1082.

Kruegel, U., Robison, B., Dange, T., Kahlert, G., Delaney, J.R., Kotireddy, S., Tsuchiya, M., Tsuchiyama, S., Murakami, C.J., Schleit, J., et al. (2011). Elevated proteasome capacity extends replicative lifespan in Saccharomyces cerevisiae. PLoS Genet. *7*, e1002253.

Kuhlbrodt, K., Janiesch, P.C., Kevei, E., Segref, A., Barikbin, R., and Hoppe, T. (2011). The Machado-Joseph disease deubiquitylase ATX-3 couples longevity and proteostasis. Nat. Cell Biol. *13*, 273–281.

Kwon, E.S., Narasimhan, S.D., Yen, K., and Tissenbaum, H.A. (2010). A new DAF-16 isoform regulates longevity. Nature *466*, 498–502.

Lam, Y.A., DeMartino, G.N., Pickart, C.M., and Cohen, R.E. (1997a). Specificity of the ubiquitin isopeptidase in the PA700 regulatory complex of 26 S proteasomes. J. Biol. Chem. *272*, 28438–28446.

Lam, Y.A., Xu, W., DeMartino, G.N., and Cohen, R.E. (1997b). Editing of ubiquitin conjugates by an isopeptidase in the 26S proteasome. Nature *385*, 737–740.

Lee, R.Y., Hench, J., and Ruvkun, G. (2001). Regulation of C. elegans DAF-16 and its human ortholog FKHRL1 by the daf-2 insulin-like signaling pathway. Curr. Biol. *11*, 1950–1957.

Lee, S.S., Kennedy, S., Tolonen, A.C., and Ruvkun, G. (2003). DAF-16 target genes that control C. elegans life-span and metabolism. Science *300*, 644–647.

Lee, B.H., Lee, M.J., Park, S., Oh, D.C., Elsasser, S., Chen, P.C., Gartner, C., Dimova, N., Hanna, J., Gygi, S.P., et al. (2010). Enhancement of proteasome activity by a small-molecule inhibitor of USP14. Nature *467*, 179–184.

Li, S., Armstrong, C.M., Bertin, N., Ge, H., Milstein, S., Boxem, M., Vidalain, P.O., Han, J.D., Chesneau, A., Hao, T., et al. (2004). A map of the interactome network of the metazoan C. elegans. Science *303*, 540–543.

Li, W., Gao, B., Lee, S.M., Bennett, K., and Fang, D. (2007). RLE-1, an E3 ubiquitin ligase, regulates C. elegans aging by catalyzing DAF-16 polyubiquitination. Dev. Cell *12*, 235–246.

Li, X., Matilainen, O., Jin, C., Glover-Cutter, K.M., Holmberg, C.I., and Blackwell, T.K. (2011). Specific SKN-1/Nrf stress responses to perturbations in translation elongation and proteasome activity. PLoS Genet. *7*, e1002119.

Libina, N., Berman, J.R., and Kenyon, C. (2003). Tissue-specific activities of C. elegans DAF-16 in the regulation of lifespan. Cell *115*, 489–502.

Lin, K., Dorman, J.B., Rodan, A., and Kenyon, C. (1997). daf-16: an HNF-3/forkhead family member that can function to double the life-span of Caenorhabditis elegans. Science *278*, 1319–1322.

Lin, K., Hsin, H., Libina, N., and Kenyon, C. (2001). Regulation of the Caenorhabditis elegans longevity protein DAF-16 by insulin/IGF-1 and germline signaling. Nat. Genet. *28*, 139–145.

Liu, G., Rogers, J., Murphy, C.T., and Rongo, C. (2011). EGF signalling activates the ubiquitin proteasome system to modulate C. elegans lifespan. EMBO J. *30*, 2990–3003.

Maeda, I., Kohara, Y., Yamamoto, M., and Sugimoto, A. (2001). Large-scale analysis of gene function in Caenorhabditis elegans by high-throughput RNAi. Curr. Biol. *11*, 171–176.

McElwee, J., Bubb, K., and Thomas, J.H. (2003). Transcriptional outputs of the Caenorhabditis elegans forkhead protein DAF-16. Aging Cell *2*, 111–121.

Mello, C.C., Kramer, J.M., Stinchcomb, D., and Ambros, V. (1991). Efficient gene transfer in C.elegans: extrachromosomal maintenance and integration of transforming sequences. EMBO J. *10*, 3959–3970.

Morley, J.F., Brignull, H.R., Weyers, J.J., and Morimoto, R.I. (2002). The threshold for polyglutamine-expansion protein aggregation and cellular toxicity is dynamic and influenced by aging in Caenorhabditis elegans. Proc. Natl. Acad. Sci. USA *99*, 10417–10422.

Morley, J.F., and Morimoto, R.I. (2004). Regulation of longevity in Caenorhabditis elegans by heat shock factor and molecular chaperones. Mol. Biol. Cell *15*, 657–664.

Murakami, Y., Matsufuji, S., Kameji, T., Hayashi, S., Igarashi, K., Tamura, T., Tanaka, K., and Ichihara, A. (1992). Ornithine decarboxylase is degraded by the 26S proteasome without ubiquitination. Nature *360*, 597–599.

Murphy, C.T., McCarroll, S.A., Bargmann, C.I., Fraser, A., Kamath, R.S., Ahringer, J., Li, H., and Kenyon, C. (2003). Genes that act downstream of DAF-16 to influence the lifespan of Caenorhabditis elegans. Nature *424*, 277–283.

Ogg, S., Paradis, S., Gottlieb, S., Patterson, G.I., Lee, L., Tissenbaum, H.A., and Ruvkun, G. (1997). The Fork head transcription factor DAF-16 transduces insulin-like metabolic and longevity signals in C. elegans. Nature *389*, 994–999.

Ohman, T., Lietzén, N., Välimäki, E., Melchjorsen, J., Matikainen, S., and Nyman, T.A. (2010). Cytosolic RNA recognition pathway activates 14-3-3 protein mediated signaling and caspase-dependent disruption of cytokeratin network in human keratinocytes. J. Proteome Res. *9*, 1549–1564.

Ovaska, K., Laakso, M., Haapa-Paananen, S., Louhimo, R., Chen, P., Aittomaki, V., Valo, E., Nunez-Fontarnau, J., Rantanen, V., Karinen, S., et al. (2010). Large-scale data integration framework provides a comprehensive view on glioblastoma multiforme. Genome Med. *2*, 65.

Pérez, V.I., Buffenstein, R., Masamsetti, V., Leonard, S., Salmon, A.B., Mele, J., Andziak, B., Yang, T., Edrey, Y., Friguet, B., et al. (2009). Protein stability and resistance to oxidative stress are determinants of longevity in the longest-living rodent, the naked mole-rat. Proc. Natl. Acad. Sci. USA *106*, 3059–3064.

Peth, A., Kukushkin, N., Bossé, M., and Goldberg, A.L. (2013). Ubiquitinated proteins activate the proteasomal ATPases by binding to Usp14 or Uch37 homologs. J. Biol. Chem. *288*, 7781–7790.

Qiu, X.B., Ouyang, S.Y., Li, C.J., Miao, S., Wang, L., and Goldberg, A.L. (2006). hRpn13/ADRM1/GP110 is a novel proteasome subunit that binds the deubiquitinating enzyme, UCH37. EMBO J. *25*, 5742–5753.

Sandri, M., Sandri, C., Gilbert, A., Skurk, C., Calabria, E., Picard, A., Walsh, K., Schiaffino, S., Lecker, S.H., and Goldberg, A.L. (2004). Foxo transcription factors induce the atrophy-related ubiquitin ligase atrogin-1 and cause skeletal muscle atrophy. Cell *117*, 399–412.

Sims, J.J., Scavone, F., Cooper, E.M., Kane, L.A., Youle, R.J., Boeke, J.D., and Cohen, R.E. (2012). Polyubiquitin-sensor proteins reveal localization and linkage-type dependence of cellular ubiquitin signaling. Nat. Methods *9*, 303–309.

Stadtmueller, B.M., and Hill, C.P. (2011). Proteasome activators. Mol. Cell *41*, 8–19.

Stitt, T.N., Drujan, D., Clarke, B.A., Panaro, F., Timofeyva, Y., Kline, W.O., Gonzalez, M., Yancopoulos, G.D., and Glass, D.J. (2004). The IGF-1/PI3K/Akt pathway prevents expression of muscle atrophy-induced ubiquitin ligases by inhibiting FOXO transcription factors. Mol. Cell *14*, 395–403.

Timmons, L., Court, D.L., and Fire, A. (2001). Ingestion of bacterially expressed dsRNAs can produce specific and potent genetic interference in Caenorhabditis elegans. Gene *263*, 103–112.

Tonoki, A., Kuranaga, E., Tomioka, T., Hamazaki, J., Murata, S., Tanaka, K., and Miura, M. (2009). Genetic evidence linking age-dependent attenuation of the 26S proteasome with the aging process. Mol. Cell. Biol. *29*, 1095–1106.

Tullet, J.M., Hertweck, M., An, J.H., Baker, J., Hwang, J.Y., Liu, S., Oliveira, R.P., Baumeister, R., and Blackwell, T.K. (2008). Direct inhibition of the longevity-promoting factor SKN-1 by insulin-like signaling in C. elegans. Cell *132*, 1025–1038.

Vandesompele, J., De Preter, K., Pattyn, F., Poppe, B., Van Roy, N., De Paepe, A., and Speleman, F. (2002). Accurate normalization of real-time quantitative RT-PCR data by geometric averaging of multiple internal control genes. Genome Biol. *3*. research0034.1–research0034.11 Published online June 18, 2002.

Vernace, V.A., Schmidt-Glenewinkel, T., and Figueiredo-Pereira, M.E. (2007). Aging and regulated protein degradation: who has the UPPer hand? Aging Cell *6*, 599–606.

Vilchez, D., Boyer, L., Morantte, I., Lutz, M., Merkwirth, C., Joyce, D., Spencer, B., Page, L., Masliah, E., Berggren, W.T., et al. (2012a). Increased proteasome activity in human embryonic stem cells is regulated by PSMD11. Nature *489*, 304–308.

Vilchez, D., Morantte, I., Liu, Z., Douglas, P.M., Merkwirth, C., Rodrigues, A.P., Manning, G., and Dillin, A. (2012b). RPN-6 determines C. elegans longevity under proteotoxic stress conditions. Nature *489*, 263–268.

Yao, T., Song, L., Xu, W., DeMartino, G.N., Florens, L., Swanson, S.K., Washburn, M.P., Conaway, R.C., Conaway, J.W., and Cohen, R.E. (2006). Proteasome recruitment and activation of the Uch37 deubiquitinating enzyme by Adrm1. Nat. Cell Biol. *8*, 994–1002.

Zarse, K., Schmeisser, S., Groth, M., Priebe, S., Beuster, G., Kuhlow, D., Guthke, R., Platzer, M., Kahn, C.R., and Ristow, M. (2012). Impaired insulin/IGF1 signaling extends life span by promoting mitochondrial L-proline catabolism to induce a transient ROS signal. Cell Metab. *15*, 451–465.

Zhao, J., Brault, J.J., Schild, A., Cao, P., Sandri, M., Schiaffino, S., Lecker, S.H., and Goldberg, A.L. (2007). FoxO3 coordinately activates protein degradation by the autophagic/lysosomal and proteasomal pathways in atrophying muscle cells. Cell Metab. *6*, 472–483.